

ANNUAL REPORT

OF THE

ERWIN L. HAHN

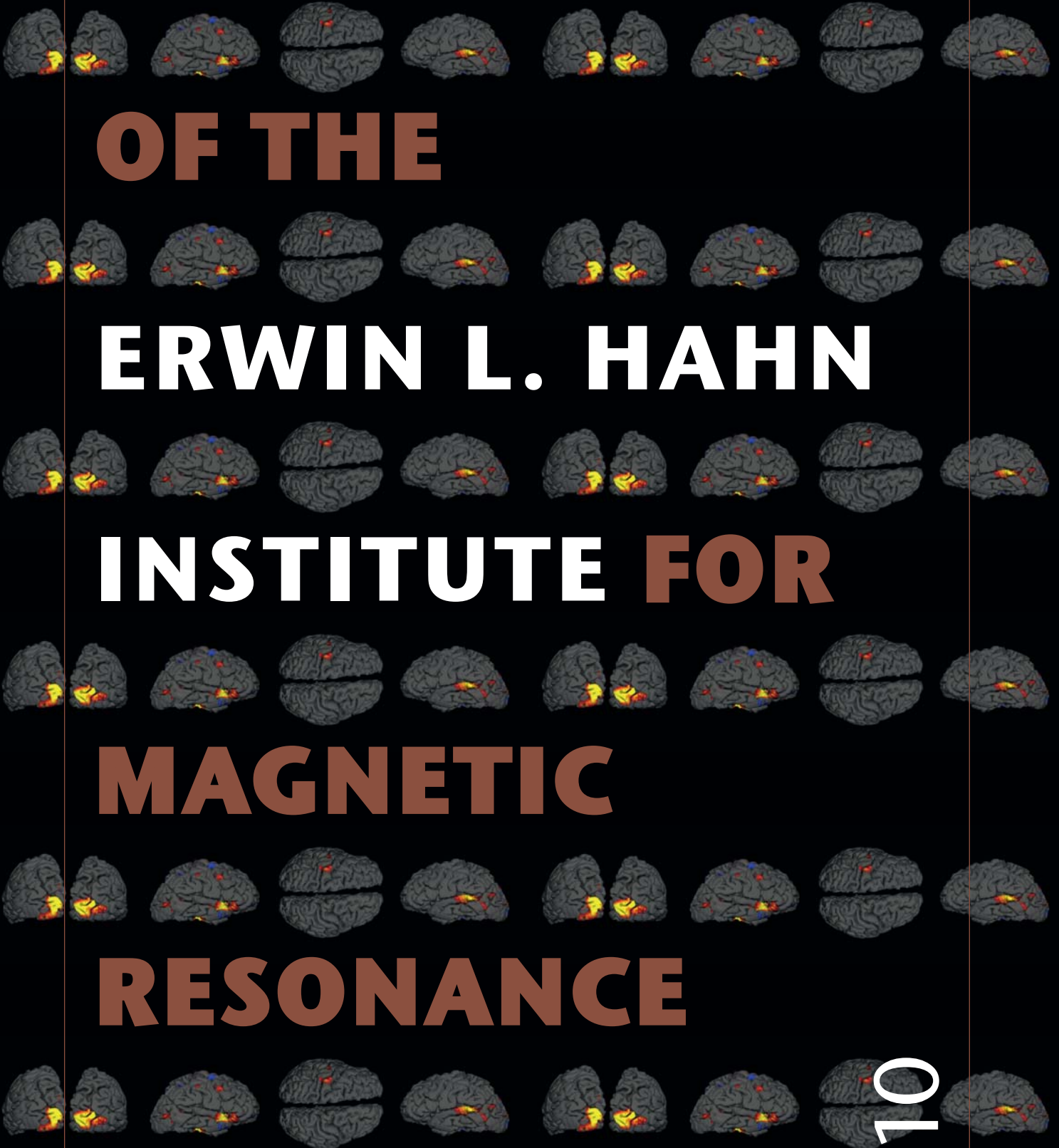
INSTITUTE FOR

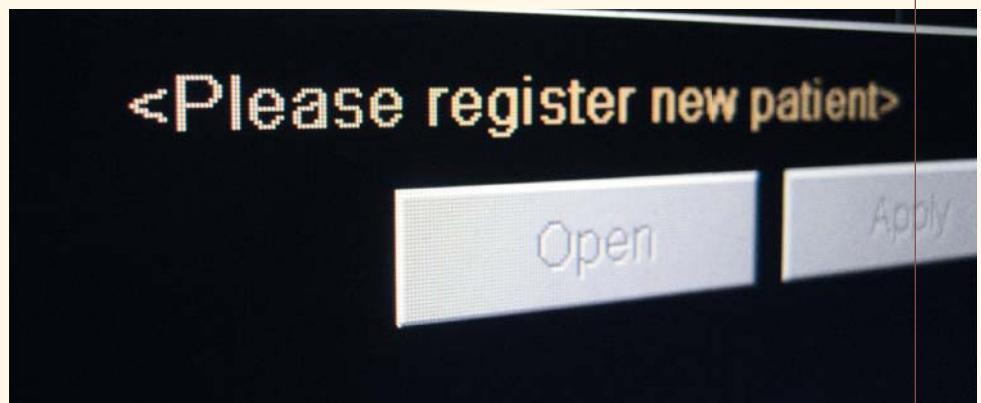
MAGNETIC

RESONANCE

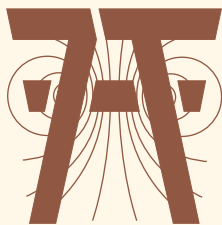
IMAGING

2010





Erwin L. Hahn Institute for Magnetic Resonance Imaging



Arendahls Wiese 199
D-45141 Essen
Germany

t ++49 (0)201-183-6070
f ++49 (0)201-183-6073
w www.hahn-institute.de

Graphic design
AMP Studio, Duisburg

Photography
All images © Erwin L. Hahn Institute



Preface

2010 was a successful one for the Erwin L. Hahn Institute. We conducted a wide range of studies and projects within several different research areas centred around MRI on a technical, fundamental basic research and clinical level. One example is the successful implementation of whole-body images resulting in a patent (TIAMO, see report by Stefan Orzada). Another example is sequence optimization for functional MRI studies on brain functions which led to impressive images of brain areas which are usually artifact-prone even at lower field strengths (see report by Schulte and Grabenhorst). These are just two examples of our successful contributions to a better understanding and improved application of 7 Tesla MRI in medical and basic research. We have also successfully installed our 32-channel head coil.

In summary, in 2010 altogether 22 manuscripts of the young and aspiring team of the Erwin L. Hahn Institute have been published in international peer-reviewed journals. In addition, over 70 talks and poster presentations at national and international conferences were held by our team members. Two young scientists received awards for their work conducted at our institute: Dr. Philipp Damman (Traugott Riechert Award of the German Society for Neurosurgery) and Oliver Kraff (Toshiba Award of the German Society of Medical Physics). We also received several new grants in 2010 (from DFG, Land NRW, Siemens, Stiftung Mercur). And our team has expanded by 11 new members in 2010.

For quality management, we have introduced a new tool for scanning time allocation. All projects running at the Erwin L. Hahn Institute are presented to the Board of Directors and team members before the project starts and finally, after completing the study, the projects are again presented and discussed. This procedure is expected to contribute to an even higher quality of studies at the institute and of publications by our team members.

Finally, we were pleased to have Prof. Eike Nagel, Professor of Clinical Cardiovascular Imaging at King's College London, as speaker at our 4th Erwin L. Hahn Lecture in November 2010. His talk demonstrated the potential and current constraints of high-field MRI techniques in cardiovascular imaging. The lecture was accompanied by lively poster presentations and interesting discussions.

In this Annual Report the reader will find additional stories of success at the Erwin L. Hahn Institute in 2010 and will hopefully be inspired to contact us for further questions and co-operations.

Matthias Brand

Essen, January 2011.



Functional brain imaging

Neural systems underlying the cost-benefit evaluation of food rewards: a 7 Tesla fMRI study

Neural mechanisms for reward valuation and value-guided, economic decision-making are central areas of investigation in cognitive neuroscience [1], [2], and functional MRI is often the tool of choice. However, the possibility of using high-field fMRI at 7T to study human valuation and choice process has been little explored so far. We conducted several studies using a custom build 8-channel transmit / receive head coil [3] as well as an optimized 7T multi-echo EPI sequence [4], both developed at the Erwin L. Hahn Institute for Magnetic Resonance Imaging, to study the operation of the brain's reward and decision systems. In the following, one of those studies is presented.

In this study, we tested whether separate parts of the brain's valuation and decision systems encode the benefits and costs of food rewards. We also investigated whether these neural representations can be selectively modulated by cognitive factors, such as word labels. Thirteen healthy and mildly hungry volunteers were asked

to evaluate pictures of food products with regard to subjective taste pleasantness, unhealthiness, and attractiveness. They also had to choose items from presented food item pairs. The food stimuli were accompanied either by a label that emphasized hedonic properties ("sweet'n'tasty"), by a label that emphasized health-related properties ("high in fat"), by both types of labels simultaneously, or by no label at all.

Neurally, we found evidence for separate encoding of subjective benefits and costs (Figure 1): Activity in medial orbitofrontal cortex produced by the food stimuli correlated with taste pleasantness (Figure 1A), activity in mid-orbitofrontal cortex correlated with food unhealthiness (Figure 1B), activity in ventral striatum correlated with food attractiveness (Figure 1C), and activity in ventromedial prefrontal cortex at the time of choice correlated with subjective decision confidence (Figure 1D). Word labels modulated neural sensitivity to benefits and costs in different brain areas.

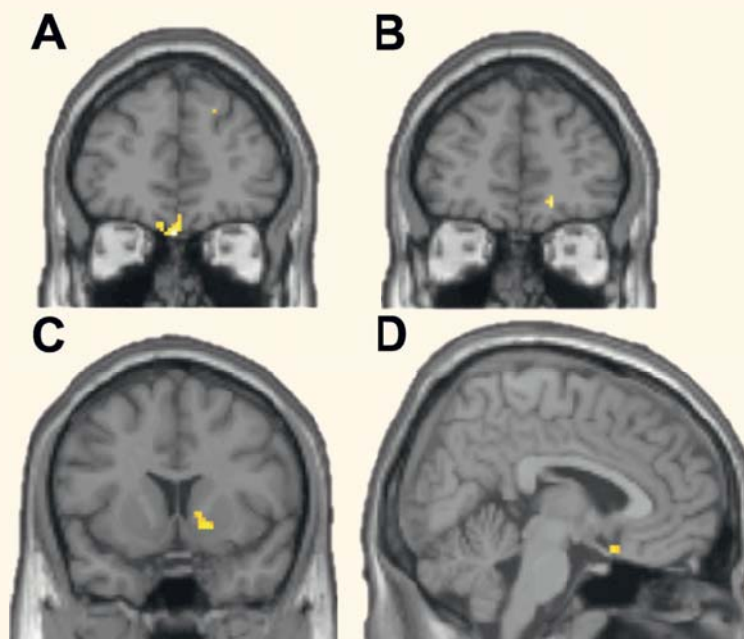


Fig. 1: Separate neural encoding of subjective benefits and costs.

Activity in the medial amygdala was more strongly correlated with taste pleasantness (food benefits) when a taste label was presented compared to when a health label was presented (Figure 2A). In converse, activity in the posterior orbitofrontal cortex/ agranular insula was more strongly correlated with unhealthiness (food costs) when a health label was presented, compared to when a taste label was presented (Figure 2B).

In summary, we found evidence for separate encoding of the subjective benefits and costs of food rewards in key structures of the brain's valuation system including different areas of the orbitofrontal cortex. We demonstrated that neural representations of the benefits and costs of rewards can be selectively influenced by word labels.

The results show that neural correlates of decision-making processes can be detected using the Erwin L. Hahn Institute's 7 Tesla MR

scanner and the imaging sequences developed here, even simultaneously in anatomically separate artifact-prone areas such as the medial orbitofrontal cortex, ventral striatum, and the amygdala. This allows us to investigate other phenomena in which frontal areas might be involved: In cooperation with the chair of Social Psychology: Media and Communication at University Duisburg-Essen (Prof. Nicole Krämer), we examine activity in frontal cortical midbrain structures in a study of self-referential processing; in other projects, we look into the neural correlates of the perception of movies which are simultaneously funny and sad, or of moral decision making.

- [1] Grabenhorst F, Rolls ET, Bilderbeck A; Cerebral Cortex. 2008, 18: 1549-1559.
- [2] Grabenhorst F, et al.; Cerebral Cortex. 2010, 20: 1082-1091.
- [3] Orzada S, et al.; ISMRM 2009, #3010.
- [4] Poser BA, et al.; Neuroimage. 2009, 1162-72.

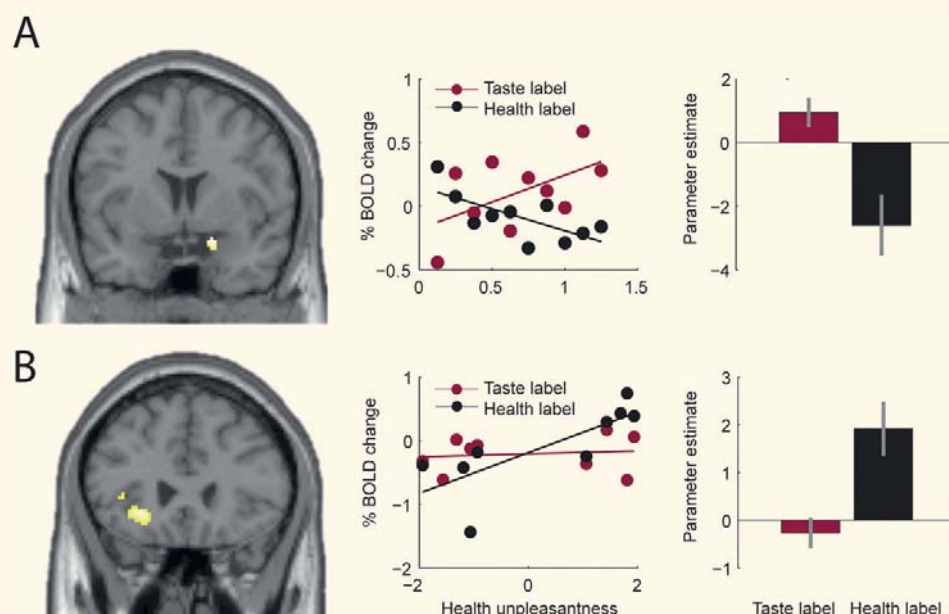


Fig. 2: Modulation of neural sensitivity to benefits and costs by word labels.

Whole-Body Imaging

A new multichannel excitation strategy enables true head-to-toe imaging at 7 Tesla

As the field strength and therefore the operational frequency in MRI is increased, the wavelength approaches the size of the human head/body, resulting in wave effects which cause signal decreases and dropouts. These signal inhomogeneities hamper the use of ultra-high field MRI systems in the human torso. Several multichannel transmit approaches have been proposed to try to tackle these problems, including RF shimming, where each element in an array is driven by its own amplifier and modulated with a certain (constant) amplitude and phase relative to the other elements, and Transmit SENSE, where spatially tailored RF pulses are used. However, these techniques

still have limitations. RF shimming using the commonly available number of 8 transmit channels has not shown satisfying results in the torso, and Transmit SENSE depends on very exact absolute B_1^+ maps, which cannot yet be reliably acquired in this body region.

At the Erwin L. Hahn Institute a relatively inexpensive and easy to use imaging scheme for 7 Tesla imaging has been developed and tested which mitigates signal voids due to transmit B_1^+ field inhomogeneity. This scheme is called “Time Interleaved Acquisition of Modes”, in short “TIAMO”.

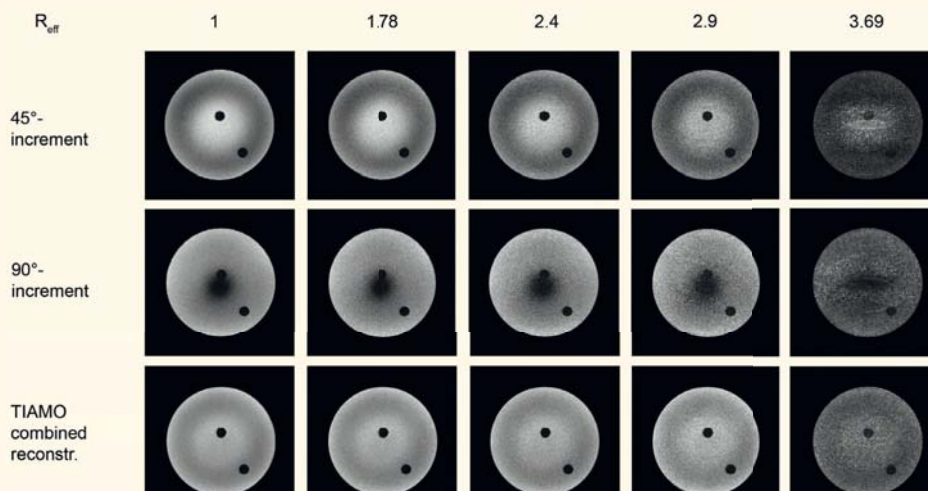


Fig. 3: 45° phase increment, 90° phase increment, and TIAMO combined reconstruction for different effective parallel imaging reduction factors. TIAMO is much more homogeneous and allows higher reduction factors. The phantom is a cylinder with two tubes (black circles) to provide some structure.

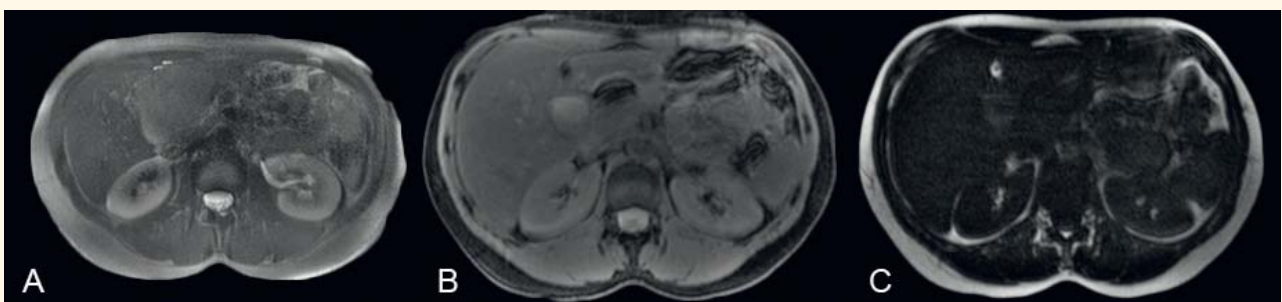


Fig. 4: (A) T2-weighted HASTE image in a human volunteer; note the absence of signal dropouts. (B) Gradient echo image with fat saturation and (C) gradient echo image with water saturation; the saturation is effective throughout the entire slice.

With this technique, two time-interleaved images are acquired using a different excitation mode for each acquisition. The calculation of these modes can be done using easy to acquire relative B_1^+ maps, and each mode does not have to be homogeneous in and of itself, but a requirement is that the signal dropouts of the modes have to be in different positions. The combination of the two images via a sum of squares method then provides a nearly homogeneous image without signal dropouts.

Unfortunately, acquiring two images doubles the acquisition time, but by forming virtual elements from the two interleaved acquisitions, this penalty in time can be significantly reduced using a GRAPPA reconstruction where the virtual elements allow a higher acceleration factor. This is demonstrated in a phantom in Figure 3, where the CP^+ mode (45° phase increment in an 8-channel head coil) and CP^{2+} mode (90° phase increment) are shown at different reduction factors as well as the TIAMO combination of the two modes which reveals a higher SNR and less pronounced acceleration artifacts.

Figure 4 shows examples from the human abdomen in the liver/kidney region. The images are homogeneous and show no signal dropouts. Figure 4A shows a T2-weighted spin echo image which is intrinsically more affected by B_1^+ inhomogeneities but is without signal dropouts owing to TIAMO. Figures 4B and 4C show gradient echo images with fat and water suppression, respectively. The saturation is effective throughout the entire slice.

In Figure 5 images from a whole-body dataset are presented. Even though a non-optimized set of modes (CP^+ and CP^{2+}) was used, the dataset is fairly homogeneous throughout the entire body, demonstrating the robustness of the method.

These results indicate that TIAMO is a very easy way to mitigate the artifacts induced by the inhomogeneity of B_1^+ at ultra-high field strengths such as 7 Tesla. First homogeneous images have been acquired, and the robustness of the method appears to make it suitable for future clinical studies.

For details of this study see Orzada S, Maderwald S, Poser BA, Bitz AK, Quick HH, Ladd ME. RF excitation using time interleaved acquisition of modes (TIAMO) to address B1 inhomogeneity in high-field MRI. *Magn Reson Med* 2010;64(2):327-333.



Fig. 5: Head-to-toe images from a human volunteer acquired with a 2.08 mm isotropic resolution. The dataset was obtained with a moving table in 28 stations. The slices are fairly homogeneous even though a non-optimized combination of the CP^+ and CP^{2+} modes was used throughout the acquisition, demonstrating the robustness of the method.

Spectroscopic imaging of X-Nuclei

Phosphorus Spectroscopy of the prostate at 7T with an endorectal coil

Nuclei other than protons (X-Nuclei) have a lower resonance frequency and an inherent lower sensitivity in magnetic resonance imaging and spectroscopy. Ultra-high magnetic field systems such as the Essen 7T whole body system have the potential to bring these lower sensitivities to a clinically acceptable level regarding temporal and spatial resolution. One of the nuclei of interest is the phosphorus atom ^{31}P , present in molecules involved in the energy metabolism of cells, and also in different molecules in membrane metabolism pathways. With ^{31}P MR spectroscopic imaging (MRSI) at 7T signals of these molecules that are present in tissues at concentrations in the millimolar range can be spatially localized with acceptable spatial and temporal resolution. Prerequisite is the combination of the ^{31}P MR coil with proton coils for accurate localisation of ^{31}P signals with regular MR images. The resulting spectra contain ^{31}P metabolic fingerprints of the tissue at hand. In the prostate, this fingerprint can be of help to discriminate between cancer and non-cancer tissue, and to determine the aggressiveness of prostate cancer, which is currently one of the most critical clinical questions in prostate cancer care.

To maximize sensitivity of the setup we designed a small loop coil, mounted inside an endorectal balloon, to transmit and receive signals at the ^{31}P frequency at 7T (120 MHz). This endorectal coil needed to be safely combined with an external 8-channel proton coil for imaging. To assure operation within safety limits, the maximum amount of power to be delivered with the endorectal coil was simulated with Finite Integration Technique (FIT) calculations in a detailed human prostate model. Moreover, power delivery and actual temperature increase

were measured in a phantom, and possible interactions between the ^{31}P endorectal coil and the external 8-channel array coil were evaluated. After safety validation, ^{31}P -MRSI of the prostate of a healthy volunteer was performed in combination with MRI of the prostate.

The RF hot spot of the ^{31}P endorectal coil design was at one of the coil capacitors, similar to an earlier design for proton signals [1], enabling independent monitoring of the temperature increase of this spot with a temperature probe during phantom examinations (Figure 6). We found a small interaction between the endorectal coil and the external 8-channel array coil in the phantom; the regular temperature increase due to power deposition with the external array coil in the known hot spots for this coil setup were larger than the locally introduced additional endorectal coil. Maximum power deposition with the external coil was therefore governed by known modelled radiofrequency patterns. After imaging of the prostate, ^{31}P -MRSI was performed with voxel sizes in the MRSI matrix of 5.8 cc in 11 minutes with a pulse-acquire pulse sequence with homogeneous signal excitation. Good ^{31}P MR spectra with high spectral resolution were obtained in the human prostate and surrounding tissues (Figure 7).

For the first time spatial variation in phosphorus spectra of the prostate and surrounding tissues is shown in vivo, detecting relevant signals involved in energy and membrane metabolism, opening up possibilities to characterize prostate cancer in the near future.

[1] Klomp DW, Bitz AK, Heerschap A, Scheenen TW. Proton spectroscopic imaging of the human prostate at 7T. *NMR Biomed.* 2009;22(5):495-501.

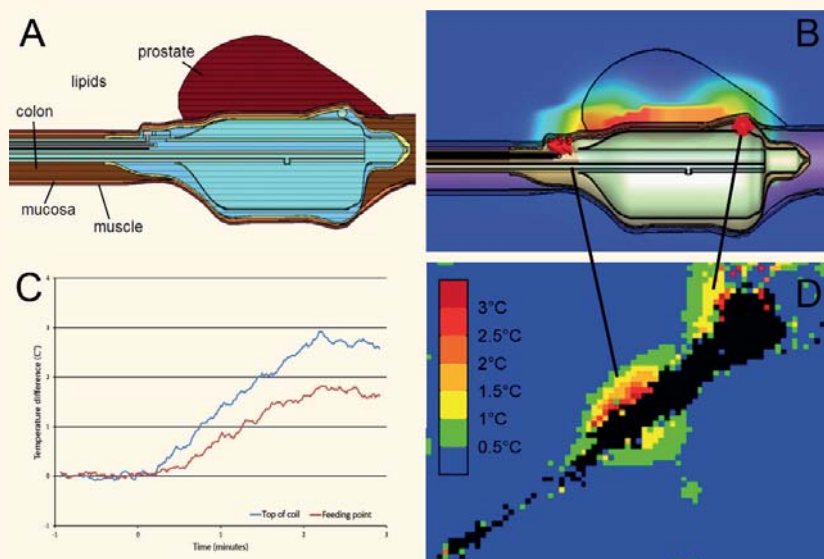
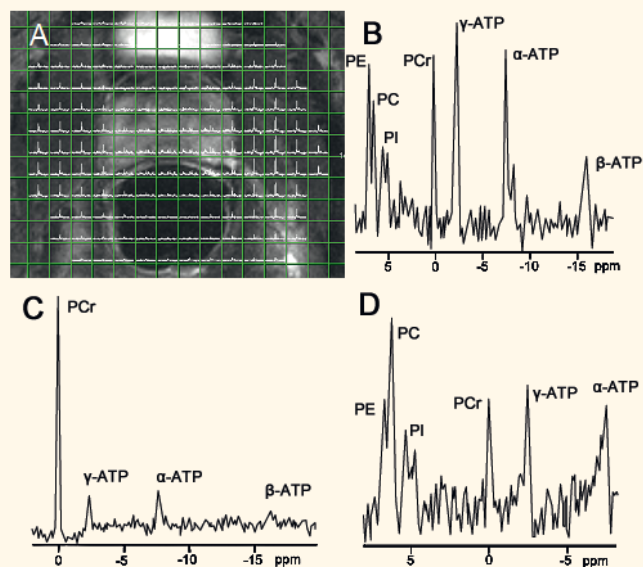


Fig. 6: SAR and temperature assessment based on simulation and phantom measurements of the endorectal ^{31}P TxRx coil. A). Detailed model of the endorectal coil, the prostate and rectum. B). The numerically calculated RF power loss density which is the source for the temperature increase over the prostate tissue model. C). True temperature increase (fiberoptic sensors) at the two hottest spots during excessive radiofrequency power deposition in a gel phantom (9.1 W in 2 minutes). D). MR thermometry of a sagittal plane

through the capacitors shows that the hottest spot in the gel phantom is closest to the capacitors positioned at the feedpoint and top of the coil. From this, maximum allowed power is 1 W for 6 minutes.

Fig. 7: ^{31}P MRSI of the prostate at 7T of a healthy volunteer showing relevant resonances at nominal voxel sizes down to 5.8 cc. A). T2 weighted axial image through the prostate, obtained with the 8-channel array coil, with ^{31}P spectra of one partition from the 3D MRSI matrix as an overlay. The prostate is in the center of the image, the bladder is the bright structure, anterior to the prostate; the rectum with endorectal coil does not have any intensity on MRI. Left and right of the prostate are smooth muscles. B). Individual ^{31}P spectra are shown from B). the prostate at midgland, C). smooth muscle next to the prostate and D). base of the prostate close to seminal vesicles. The following metabolites were observed: phosphocreatine (PCr), inorganic phosphate (Pi), adenosine triphosphate (ATP), phosphoethanolamine (PE) and phosphocholine (PC).



Functional imaging of Cortical Layers

A handle on brain information flow

The quality of MR images expressed in terms of signal-to-noise ratio (SNR) scales with magnetic field strength. The superior SNR provided by a 7 Tesla system allows depiction of very fine structures in the human brain, features that would not be detectable at lower field strengths. Examples of such structures are the cortical layers. Highly simplified, the brain can be seen as a ball of so-called white matter (WM) covered in a sheet of grey matter (GM). Grey matter contains the neurons that perform all of our brain's calculations whereas white matter serves as the "wiring" which transports the signals from one brain area to another. The sheet of grey matter is called the (neo)cortex and is, on average, 3 mm thick. In the early 1990s it was discovered that the neuronal activity in the cortex could be detected in MRI scanners (a technique dubbed functional MRI, or fMRI). Ever since,

neuroscientists have extensively mapped the human brain resulting in detailed knowledge of which area does what.

Now most areas have been assigned a function, the focus of fMRI has shifted to the investigation of brain networks: how is the information flow organized? One handle on this can potentially be found in the internal organization of the cortex. As shown in Figure 8a, the cortex consists of multiple histologically distinct layers. These layers have different roles in terms of input, output and feedback etc. as can be seen in Figure 8b which shows the direction of information flow. However, as mentioned earlier, the entire cortex (i.e. all layers together) is only 3 mm thick which is roughly equal to the level of detail visible in conventional (low field) fMRI. The superior sensitivity of the 7 Tesla scanner

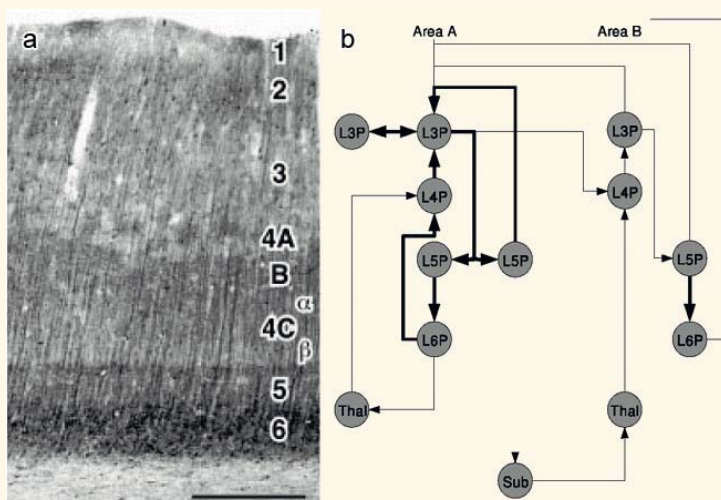


Fig. 8: The Structure of neocortex
8a: A microscopy image of the human cortex after staining clearly show a layered organization. (Figure adapted from: Preuss et al., PNAS 1999)
8b: Flowchart of neuronal processing as reported by ex-vivo tracing studies. It describes the roles of the different layers. Input coming from the thalamus arrives in layer 4 for instance (Thal -> L4P). Current research goals are to try and measure such schemes in-vivo with fMRI. (Figure taken from: Douglas and Martin, Ann. Rev. Neurosc. 2004)



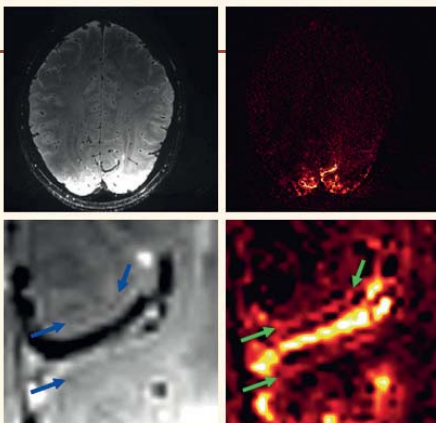
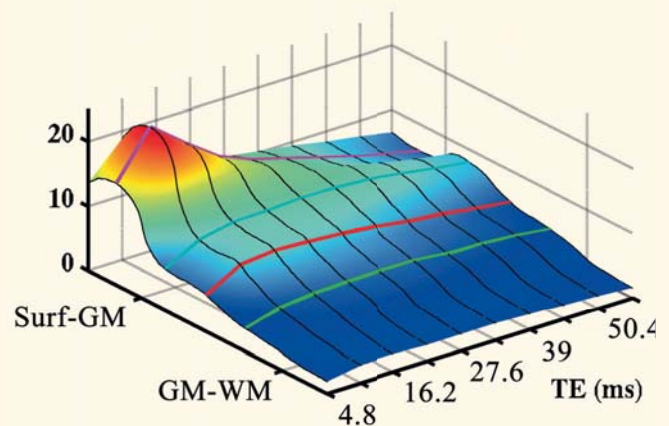


Fig. 9: High resolution 7T fMRI images of the visual cortex. The left column shows a single brain image at the top, with a zoomed section of the visual cortex below. The blue arrows point out a dark line called “stripe of Gennari” which is located in layer 4. On the right functional activation is shown (the response of visual cortex to a flickering screen stimulus). The strongest activation (yellow) is seen in the blood vessels at the surface (see also Figure 10) but one can also see that layer 4 activates (green arrows) more strongly than its neighbouring layers.

Fig. 10: Activation of cortical layers versus scan parameters. fMRI activation patterns can be dependent on certain scan parameters, the most influential one being the “echo time” (TE). Figure 10 shows the activation strength at each cortical depth (layer 6 is close to the GM-WM boundary, layer 1 is just below the surface). Here one can see that choosing a short TE results in images that show a strong activation in the surface veins (the big red peak). Scans with a long TE on the other hand are more sensitive to activation in layers 2-3. Such information is crucial when interpreting layer-specific fMRI data.



together with dedicated RF coils developed at the Erwin L. Hahn institute made possible one of the first fMRI studies at the level of the cortical layers, results of which are shown in Figures 9 and 10. This proof-of-principle study showed it is possible to acquire layer-specific fMRI signals thus providing large potential for brain network analyses.

Layer-specific fMRI in practice

For layer-specific fMRI to work two main points must be met:

- The fMRI data have to have a very high spatial resolution as differences in cortical depth have to be discerned which are on sub-millimetre scale

- To determine cortical depth, highly accurate knowledge of the cortical boundaries is needed, i.e. where is the WM-GM boundary, where is the cortical surface?

To meet these demands, functional data were acquired with a resolution of $0.75 \times 0.75 \times 0.75 \text{ mm}^3$, which is approximately 100x smaller than the volume of an image element in a conventional fMRI experiment. Also, a T_1 -weighted acquisition was performed with the same resolution which provides high contrast between WM and GM tissue. This provided detailed knowledge on the GM boundaries. By resampling the acquired fMRI images perpendicularly from the WM-GM boundary to the cortical surface, depth dependent activation profiles as shown in Figure 10 were produced.

4th Erwin L. Hahn Lecture



Young scientists at the poster session



The lecture



New scientists in 2010



Happy at the end



Current Grants

Bayer P, Hoffmann D, Haberhauer G, Ladd ME, Eggert A, Schramm A, Arndt M, Krauss J. ModularProbes: Structure based design of modular MRI probe molecules for the highly sensitive detection of metastases. German Federal Ministry of Education and Research; duration: 3 years (January 2009 – December 2011)

Winterhager E, Gruemmer R, Ladd ME. Effects of repeated exposure to strong static magnetic fields from magnetic resonance imagers on the endpoints reproduction and development in an animal model. German Federal Office for Radiation Protection; duration: 3 years (April 2008 – March 2011)

Bahr A, Ladd ME, Solbach K, Lehmkuehler O. 7-Tesla MRI body coil – multichannel transmit techniques and strategies for high-field magnetic resonance imaging. German Federal Ministry of Education and Research; duration 3 years (July 2007 – June 2010)

Ladd ME, Forsting M, Ladd SG. Prevalence, co-morbidity and risk factors on non-Alzheimer dementia. Jackstädt Foundation; duration 5 years (October 2005 – June 2010)

Rennings A, Erni D, Ladd ME, Quick HH, Solbach K, Otto S. Competition Science-to-Business PreSeed: MetaCoils – Metamaterial-based high-frequency-coils for 7-Tesla-MRI; duration 2 years (May 2010 – April 2012)

Brand M, Wolf OT. Stress and risky decisions – behavioral, neuroendocrine and neural correlates of the interaction of stress, executive functions and decision making in risky situations. German Research Foundation; duration 2 years (October 2010 - September 2012)

Personnel

New in 2010

Simone Brunn
Dr. phil. (Oxford) Fabian Grabenhorst
Dr. med. Dagny Holle
Sören Johst
Yacine Nouredine
Mirko Pawlikowski
Dr. rer. nat. Frank P. Schulte
Bettina Staschkiewicz
Roxana Stefanescu
Dr. med. Lale Umutlu
Dr. med. Karsten Wrede

Left in 2010

Dr. med. Philipp Dammann
Dr. scient. Pål E. Goa
Manuela Mondry
Dr. rer. nat. Benedikt Poser

Publications

Kraff O, Bitz AK, Dammann P, Ladd SC, Ladd ME, Quick HH. *An eight-channel transmit/receive multi-purpose coil for musculoskeletal MR imaging at 7 Tesla*. Medical Physics, December 2010; 37(12): 6368-6376.

Küper M, Dimitrova A, Thürling M, Maderwald S, Roths J, Elles HG, Gizewski ER, Ladd ME, Diedrichsen J, Timmann D. *Evidence for a motor and a non-motor domain in the human dentate nucleus - an fMRI study*. Neuroimage. 2010 Nov 13.

Diedrichsen J, Maderwald S, Küper M, Thürling M, Rabe K, Gizewski ER, Ladd ME, Timmann D. *Imaging the deep cerebellar nuclei: A probabilistic atlas and normalization procedure*. Neuroimage. 2010 Oct 18.

Umutlu L, Orzada S, Kinner S, Maderwald S, Brote I, Bitz AK, Kraff O, Ladd SC, Antoch G, Ladd ME, Quick HH, Lauenstein TC. *Renal imaging at 7 Tesla: preliminary results*. Eur Radiol. 2010 Sep 25.

Dammann P, Barth M, Zhu Y, Maderwald S, Schlamann M, Ladd ME, Sure U. *Susceptibility weighted magnetic resonance imaging of cerebral cavernous malformations: prospects, drawbacks, and first experience at ultra-high field strength (7-Tesla) magnetic resonance imaging*. Neurosurg Focus. 2010 Sep;29(3):E5. Review.

Noebauer-Huhmann IM, Szomolanyi P, Juras V, Kraff O, Ladd ME, Trattnig S. *Gadolinium-based magnetic resonance contrast agents at 7 Tesla: in vitro T1 relaxivities in human blood plasma*. Invest Radiol. 2010 Sep;45(9):554-8

Mönninghoff C, Maderwald S, Theysohn JM, Schütt P, Gauler T, Kraff O, Ladd ME, Ladd SC, Wanke I. *Imaging of brain metastases of bronchial carcinomas with 7 T MRI - initial results*. Rofo. 2010 Sep;182(9):764-72.

Umutlu L, Maderwald S, Kraff O, Theysohn JM, Kuemmel S, Hauth EA, Forsting M, Antoch G, Ladd ME, Quick HH, Lauenstein TC. *Dynamic contrast-enhanced breast MRI at 7 Tesla utilizing a single-loop coil: a feasibility trial*. Acad Radiol. 2010 Aug;17(8):1050-6.

Orzada S, Maderwald S, Poser BA, Bitz AK, Quick HH, Ladd ME. *RF excitation using time interleaved acquisition of modes (TIAMO) to address B1 inhomogeneity in high-field MRI*. Magn Reson Med. 2010 Aug;64(2):327-33.

Grabner G, Trattnig S, Barth M. *Filtered deconvolution of a simulated and an in vivo phase model of the human brain*. J Magn Reson Imaging. 2010 Aug;32(2):289-97.

Küper M, Thürling M, Maderwald S, Ladd ME, Timmann D. *Structural and Functional Magnetic Resonance Imaging of the Human Cerebellar Nuclei*. Cerebellum. 2010 Jul 28.

- Poser BA, Norris DG. *Application of whole-brain CBV-weighted fMRI to a cognitive stimulation paradigm: Robust activation detection in a stroop task experiment using 3D GRASE VASO*. Hum Brain Mapp. 2010 Jun 24.
- Orzada S, Maderwald S, Göricke SL, Parohl N, Ladd SC, Ladd ME, Quick HH. *Design and comparison of two eight-channel transmit/receive radiofrequency arrays for in vivo rodent imaging on a 7 T human whole-body MRI system*. Med Phys. 2010 May;37(5):2225-32.
- Poser BA, Koopmans PJ, Witzel T, Wald LL, Barth M. *Three dimensional echo-planar imaging at 7 Tesla*. Neuroimage. 2010 May 15;51(1):261-6.
- Schlamann M, Voigt MA, Maderwald S, Bitz AK, Kraff O, Ladd SC, Ladd ME, Forsting M, Wilhelm H. *Exposure to high-field MRI does not affect cognitive function*. J Magn Reson Imaging. 2010 May;31(5):1061-6.
- Poser BA, van Mierlo E, Norris DG. *Exploring the post-stimulus undershoot with spin-echo fMRI: Implications for models of neurovascular response*. Hum Brain Mapp. 2010 Apr 16.
- Breyer T, Wanke I, Maderwald S, Woermann FG, Kraff O, Theysohn JM, Ebner A, Forsting M, Ladd ME, Schlamann M. *Imaging of patients with hippocampal sclerosis at 7 Tesla: initial results*. Acad Radiol. 2010 Apr;17(4):421-6.
- Moenninghoff C, Kraff O, Schlamann M, Ladd ME, Katsarava Z, Gizewski ER. *Assessing a dysplastic cerebellar gangliocytoma (Lhermitte-Duclos disease) with 7T MR imaging*. Korean J Radiol. 2010 Mar;11(2):244-8.
- Moenninghoff C, Maderwald S, Theysohn JM, Kraff O, Ladd ME, El Hindy N, van de Nes J, Forsting M, Wanke I. *Imaging of adult astrocytic brain tumours with 7 T MRI: preliminary results*. Eur Radiol. 2010 Mar;20(3):704-13.
- Schlamann M, Yoon MS, Maderwald S, Pietrzyk T, Bitz AK, Gerwig M, Forsting M, Ladd SC, Ladd ME, Kastrup O. *Short term effects of magnetic resonance imaging on excitability of the motor cortex at 1.5T and 7T*. Acad Radiol. 2010 Mar;17(3):277-81.
- Schlamann M, Maderwald S, Becker W, Kraff O, Theysohn JM, Mueller O, Sure U, Wanke I, Ladd ME, Forsting M, Schaefer L, Gizewski ER. *Cerebral cavernous hemangiomas at 7 Tesla: initial experience*. Acad Radiol. 2010 Jan;17(1):3-6.
- Ladd ME, Timmann D, Gizewski ER. *Ultrahochfeld-MRT in der Neurologie [Ultra-High-Field MRI in Neurology]*. Aktuelle Neurologie. 2010;37:219-230.



ERWIN L. HAHN
INSTITUTE
FOR
MAGNETIC
RESONANCE
IMAGING

PARTICIPATING INSTITUTIONS

UNIVERSITÄT
**DUISBURG
ESSEN**

FAKULTÄT FÜR
INGENIEURWISSENSCHAFTEN



Universitätsklinikum Essen

Radboud University Nijmegen



UMC  **St Radboud**

Donders Institute
for Brain, Cognition and Behaviour

